

Chandra detection of a parsec scale wind in the Broad Line Radio Galaxy 3C 382

J. N. Reeves

Astrophysics Group, School of Physical & Geographical Sciences, Keele University, Keele, Staffordshire ST5 5BG, UK; e-mail jnr@astro.keele.ac.uk

R. M. Sambruna

NASA/GSFC, Code 662, Greenbelt, MD 20771, USA

V. Braitto

University of Leicester, Department of Physics & Astronomy, University Road, Leicester LE1 7RH, UK

Michael Eracleous

Department of Astronomy & Astrophysics and Center for Gravitational Wave Physics, The Pennsylvania State University, 525 Davey Laboratory, University Park, PA 16802, USA

ABSTRACT

We present unambiguous evidence for a parsec scale wind in the Broad-Line Radio Galaxy (BLRG) 3C 382, the first radio-loud AGN, with $R_L = \log_{10}(f_{5\text{GHz}}/f_{4400}) > 1$, whereby an outflow has been measured with X-ray grating spectroscopy. A 118 ks Chandra grating (HETG) observation of 3C 382 has revealed the presence of several high ionization absorption lines in the soft X-ray band, from Fe, Ne, Mg and Si. The absorption lines are blue-shifted with respect to the systemic velocity of 3C 382 by $-840 \pm 60 \text{ km s}^{-1}$ and are resolved by Chandra with a velocity width of $\sigma = 340 \pm 70 \text{ km s}^{-1}$. The outflow appears to originate from a single zone of gas of column density $N_{\text{H}} = 1.3 \times 10^{21} \text{ cm}^{-2}$ and ionization parameter $\log(\xi/\text{erg cm s}^{-1}) = 2.45$. From the above measurements we calculate that the outflow is observed on parsec scales, within the likely range from 10 – 1000 pc, i.e., consistent with an origin in the Narrow Line Region.

Subject headings: Galaxies: active — galaxies: individual (3C 382)— X-rays: galaxies

1. Introduction

At least 50% of radio-quiet AGN exhibit evidence for photoionized outflows in their X-ray spectra (Reynolds 1997; George et al. 1998; Crenshaw et al. 2003; Porquet et al. 2004; Blustin et al. 2005; McKernan et al. 2007). The signatures of these winds consist of absorption and emission features at soft (0.4–2 keV) and hard (6–8 keV) X-ray energies, coincident with ionized O, N, Ne, Mg, Si and Fe lines blueshifted in the observer’s rest-frame. The inferred velocities of the winds are typically in the range 100 – 1000 km s⁻¹, but can be as high as $\sim 0.1c$ in some sources (Chartas et al. 2002, 2003; Pounds et al. 2003; Reeves et al. 2003, 2008). It is also possible that the energy budget of the outflows of some AGN can approach a significant fraction of the bolometric or even Eddington luminosity (King & Pounds 2003).

In stark contrast, the X-ray evidence for nuclear outflows is very scarce in Broad-Line Radio Galaxies (BLRGs) and in radio-loud AGN generally. Previously, the radio-loud quasar 4C +74.26 showed weak absorption features at ~ 1 keV with *ASCA* (Ballantyne 2005), while the BLRG Arp 102B showed neutral X-ray absorption with *ASCA* and a UV outflow of a few hundred km s⁻¹ (Eracleous et al. 2003). Furthermore two radio galaxies, 3C 445 and 3C 33 (Sambruna et al. 2007; Evans et al. 2006) also exhibit soft X-ray emission lines below 2 keV, which could originate from spatially extended material (in 3C 33; Torresi et al. (2009a)). Disk winds are also expected in radio-loud AGN as ingredients for jet formation (Blandford & Payne 1982).

To differentiate between radio-loud and radio-quiet AGN, here we adopt the radio-loudness parameter $R_L = \log_{10}(f_{5\text{GHz}}/f_{4400})$, where $f_{5\text{GHz}}$ is the core 5 GHz radio flux and f_{4400} is the flux at 4400Å, both in units of mJy (Kellerman et al. 1989). Generally, $R_L > 1$ for radio-loud AGN (Wilkes & Elvis 1987), while for 3C 382, $R_L = 1.9$ (Lawson & Turner 1997). If the extended radio emission from 3C 382 is also included, then R_L may be considerably higher.

In this Letter we present direct evidence for outflowing gas from the nucleus of the nearby ($z = 0.05787$), bright BLRG 3C 382. A re-analysis of our 118 ks *Chandra* HETG (High Energy Transmission Grating) observations (Gliozzi et al. 2007) revealed several blueshifted absorption lines between 0.7 – 2.0 keV which suggest the presence of a large-scale (10 – 1000 pc) outflow in this source with a velocity of 800 km s⁻¹. The organization of this Letter is as follows. In § 2 we describe the *Chandra* data reduction and analysis; in § 3 the results of the spectral analysis; Discussion and Conclusions follow in § 4. Throughout this paper, a concordance cosmology with $H_0 = 71$ km s⁻¹ Mpc⁻¹, $\Omega_\Lambda=0.73$, and $\Omega_m=0.27$ (Spergel et al. 2003) is adopted. Errors are quoted to 90% confidence for 1 parameter of interest (i.e. $\Delta\chi^2$ or $\Delta C = 2.71$).

2. The Chandra HETG Data

Chandra observed 3C 382 with the HETG for a net exposure of 118 ks between 27–30 November 2005. The ± 1 order spectra were summed for the MEG (Medium Energy Grating) and HEG (High Energy Grating) respectively, along with their response files. The summed first order count rates for the MEG and HEG are $0.867 \text{ counts s}^{-1}$ and $0.379 \text{ counts s}^{-1}$ respectively, while the MEG data were fitted between 0.5–7.0 keV and the HEG from 1.0–9.0 keV.

3. The Warm Absorber in 3C 382

The *Chandra* HETG data were first analyzed by Gliozzi et al. (2007), who focused on the continuum and its variability. Our results are in agreement with theirs. Specifically, the MEG and HEG data were fitted by an absorbed power law with photon index $\Gamma = 1.66 \pm 0.01$ plus a blackbody with $kT = 92 \pm 6 \text{ eV}$ to parameterize the soft excess below 1 keV (Gliozzi et al. 2007), absorbed by a Galactic line of sight column of $N_{\text{H,Gal}} = 7.0 \times 10^{20} \text{ cm}^{-2}$ (Dickey & Lockman 1990). Figure 1 shows the broad-band HETG spectrum fitted with an absorbed power-law only, to illustrate that a soft excess is clearly present below 1 keV. The 0.5–9 keV band flux is $6.4 \times 10^{-11} \text{ erg cm}^{-2} \text{ s}^{-1}$. Even upon adding a blackbody to parameterize the soft excess, the fit is still formally unacceptable ($\chi^2/\text{dof} = 632/477$, null probability 2.4×10^{-6}) as there are clear residuals around 1 keV that indicate the presence of a warm absorber.

To analyse the warm absorber in detail, the HEG and MEG spectra were binned more finely to sample the resolution of the detector, at approximately HWHM the spectral resolution (e.g. $\Delta\lambda = 0.01 \text{ \AA}$ bins for the MEG). For the fits, the C-statistic was used (Cash 1979), as there are fewer than 20 counts per resolution bin. The absorption lines were modelled with Gaussian profiles and the continuum model was adopted from above. Table 1 lists the detected lines with their observed and inferred properties, and their significance as per the C-statistic. Figure 2 shows the portions of the HETG spectrum containing the strongest lines, with the model overlaid.

The seven absorption lines in Table 1 and Figure 2 are all detected at high confidence (corresponding to $\Delta C > 18$, or $> 99.9\%$ confidence for 2 parameters of interest). The lines likely arise from the $1s - 2p$ transitions of Ne IX, Ne X, Si XIII, and Si XIV and the $2p - 3d$ lines of Fe XIX–XXI. The two statistically weaker $1s - 2p$ lines of Mg XI and Mg XII may also be present, which have outflow velocities consistent with the other lines.

Initially we assume that the lines have the same velocity width within the errors. The velocity width of the absorption lines is then $\sigma = 340 \pm 70 \text{ km s}^{-1}$ (or $780 \pm 160 \text{ km s}^{-1}$ FWHM)

and the lines are clearly resolved. Even at 99% confidence ($\Delta C = 9.2$ for 2 parameters), the velocity width is constrained to $\sigma = 340 \pm 140 \text{ km s}^{-1}$. Upon allowing the velocity width of the individual lines to vary, then they are constrained to lie within the range $\sigma = 250 - 500 \text{ km s}^{-1}$ as shown in Table 1. The mean outflow velocity is -810 km s^{-1} . The overall fit statistic is $C = 3804$ for 3811 bins.

We used the photoionization code XSTAR (Kallman et al. 2004) to derive the parameters of the absorber, assuming the baseline continuum described above, including the soft excess. Solar abundances are assumed throughout (Grevesse & Sauval 1998). An important input parameter is the turbulent velocity, which can effect the absorption line equivalent widths and hence the derived column density. We experimented with two different values of the turbulent velocity chosen to represent two likely extremes: (i) a lowest value of $v_{\text{turb}} = 100 \text{ km s}^{-1}$ and (ii) $v_{\text{turb}} = 300 \text{ km s}^{-1}$, the latter being consistent with the measured width of the absorption lines. The fitted continuum parameters are $\Gamma = 1.68 \pm 0.02$ and for the blackbody, $kT = 110 \pm 8 \text{ eV}$. For case (i), then $N_{\text{H}} = (3.2 \pm 0.6) \times 10^{21} \text{ cm}^{-2}$, the ionization parameter is $\log \xi^1 = 2.45_{-0.08}^{+0.13}$ and the outflow velocity is $v_{\text{out}} = -810_{-55}^{+60} \text{ km s}^{-1}$. The fit statistic is $C/\text{bins} = 3795/3811$. For case (ii), then $N_{\text{H}} = (1.30 \pm 0.25) \times 10^{21} \text{ cm}^{-2}$, $\log \xi = 2.45_{-0.07}^{+0.06}$ and the outflow velocity $v_{\text{out}} = -840_{-50}^{+60} \text{ km s}^{-1}$. The fit statistic is $C/\text{bins} = 3783/3811$. If the warm absorber is not included in the model, then the fit statistic is substantially worse by $\Delta C = 220$ (compared to model (ii)). Only a single outflowing layer of gas is required to model the warm absorber.

The higher turbulence velocity model is statistically preferred and is consistent with the measured 340 km s^{-1} widths of the lines. Either model yields an outflow velocity of -800 km s^{-1} within a statistical error of $< 10\%$. Hereafter we adopt the parameters from model (ii), as the turbulent velocity is consistent with widths of the individual absorption lines. However in neither model is the fitted column density of the absorber as high as the value of $N_{\text{H}} \sim 3 \times 10^{22} \text{ cm}^{-2}$ reported by Torresi et al. (2009b) from an analysis of a short 34.5 ks XMM-Newton/RGS observation of 3C 382 on April 28, 2008. If the column density of the warm absorber is fixed to the value of $N_{\text{H}} = 3 \times 10^{22} \text{ cm}^{-2}$ in the HETG spectrum, then the fit statistic is considerably worse ($C/\text{bins} = 8390/3811$).

As a consistency check, we analyzed the archival RGS data of 3C 382 with model (ii) and the same continuum form as above. We found that the column density and ionization parameter were degenerate with each other, given the short exposure of the RGS spectrum. Thus for the RGS, $N_{\text{H}} = 1.4_{-1.3}^{+1.4} \times 10^{22} \text{ cm}^{-2}$, $\log \xi = 3.4 \pm 1.0$ and the outflow velocity $v_{\text{out}} = -1200_{-500}^{+300} \text{ km s}^{-1}$. The fit statistic improves only by $\Delta C = 25$ to $C/\text{bins} = 826/820$

¹The units of ξ are erg cm s^{-1} .

upon adding the absorber. Thus within the larger errors, the parameters are consistent with those obtained from the HETG. The individual lines detected in the Chandra HETG observation were also compared to the absorption lines claimed by Torresi et al. (2009b) on the basis of the RGS data. With the higher signal to noise ratio of the HETG spectrum compared to the RGS spectrum, we only confirm the detection of one line reported by Torresi et al. (2009b), the Fe xx line at a rest-frame energy of 1025 eV²

4. Discussion and Conclusions

The Chandra HETG spectra have revealed an ionized outflow in the BLRG 3C 382. The outflow parameters are well determined, with $N_{\text{H}} = (1.30 \pm 0.25) \times 10^{21} \text{ cm}^{-2}$, $\log \xi = 2.45_{-0.07}^{+0.06}$ and $v_{\text{out}} = -840_{-50}^{+60} \text{ km s}^{-1}$, while the absorption line widths are resolved with $\sigma = 340 \pm 70 \text{ km s}^{-1}$.

To characterize the outflow, we define the (unabsorbed) ionizing luminosity L_{ion} , which in XSTAR is defined from 1 – 1000 Rydberg. This depends on the continuum model fitted to the data and it is important to take into account the soft excess. Using the best fit powerlaw plus blackbody continuum, then $L_{\text{ion}} = 1.2 \times 10^{45} \text{ erg s}^{-1}$. We note that if a different continuum form is used to parameterize the soft excess, e.g. a broken power-law, then the ionizing luminosity can be a factor of ~ 2 higher; keeping this caveat in mind we adopt the more conservative lower luminosity value of $1.2 \times 10^{45} \text{ erg s}^{-1}$

4.1. The Location of the Absorber

The upper-bound to the wind radius (R_{out}) is determined by geometrical constraints, i.e. if the thickness of the absorber $\Delta R/R \ll 1$ (valid for a thin shell) and as $N_{\text{H}} = n\Delta R$, where n is the electron number density. As the ionization parameter of the absorber is defined as $\xi = L_{\text{ion}}/nR^2$, then by substitution $R_{\text{out}} \ll L_{\text{ion}}/N_{\text{H}}\xi = 3.3 \times 10^{21} \text{ cm}$ (or $\ll 1 \text{ kpc}$)³. The lower bound is formed by the escape velocity, i.e. for the gas to escape the system as an outflow then $R_{\text{esc}} > c^2/v^2 R_{\text{s}}$, where $R_{\text{s}} = 2GM/c^2$ is the black hole Schwarzschild radius and $v = 800 \text{ km s}^{-1}$. If for 3C 382, $M = 1 \times 10^9 M_{\odot}$ (with a 40% uncertainty, see Marchesini et al. (2004)), then $R_{\text{esc}} > 1.4 \times 10^5 R_{\text{s}} > 4.2 \times 10^{19} \text{ cm} > 13 \text{ pc}$. In other words the location of the

²The line reported at 1.356 keV by Torresi et al. (2009b) may also be associated with the $1s - 2p$ line of Mg XI, as noted in Table 1.

³Note the same radius is obtained by integrating down the line of sight of a homogeneous radial outflow.

soft X-ray outflow is likely bounded between approximately 10 pc and 1 kpc.

Furthermore the outflow velocity and absorption line FWHM of $\sim 800 \text{ km s}^{-1}$ is similar to the width of the narrow optical forbidden lines of [O III], [O I] and [Si II], which for 3C 382 lie in the range $400 - 600 \text{ km s}^{-1}$, as measured from the spectra of Eracleous & Halpern (1994). In particular the [O III] emission line from the Eracleous & Halpern (1994) spectrum appears to have an asymmetric profile, with the blue-wing extending to $\sim -1070 \text{ km s}^{-1}$ from the line centroid, which appears $\sim 370 \text{ km s}^{-1}$ broader than the red-wing.

Although this is not evidence for observing outflowing gas through the direct line of sight, the [O III] emission may suggest we are viewing outflowing gas along a different sight-line. Indeed this effect is also seen in other radio galaxies (Gelderman & Whittle 1994). The coincidence between the soft X-ray absorbing gas and extended [O III] emission has also been noted in the radio-quiet quasar, MR 2251-178 (Kaspi et al. 2004). Thus the origin of the X-ray absorption appears consistent with the optical Narrow Line Region (NLR). The association between the soft X-ray absorption in 3C 382 and any rest-frame UV absorption could be tested with future simultaneous Chandra and HST observations.

The density of the outflow is then $n = L_{\text{ion}}/\xi R^2$. For the parameters above, then $n = 0.4 - 2400 \text{ cm}^{-3}$. While loosely constrained, this is consistent with typical expected NLR densities of $\sim 10^3 \text{ cm}^{-3}$ in AGN (Koski 1978). The mass outflow rate for a uniform spherical flow is $\dot{M}_{\text{out}} = 4\pi n R^2 m_p v_{\text{out}}$, where $n R^2 = L_{\text{ion}}/\xi$ and m_p is the proton mass. Hence for the measured warm absorber parameters for 3C 382, $\dot{M}_{\text{out}} = 7.2 \times 10^{27} \text{ g s}^{-1}$ or $\dot{M}_{\text{out}} = 100 M_{\odot} \text{ yr}^{-1}$.

However the low rate of appearance of such absorbers amongst BLRG's or radio-loud AGN generally might suggest that the solid angle subtended by individual absorbing filaments is much smaller than 4π steradians. Therefore, the mass outflow rate could be considerably smaller than the above estimate. Subsequently the kinetic power of the soft X-ray outflow (for $v_{\text{out}} = -800 \text{ km s}^{-1}$) is then $\dot{E} = 1/2 \dot{M}_{\text{out}} v_{\text{out}}^2 < 2 \times 10^{43} \text{ erg s}^{-1}$, which energetically is a fairly insignificant 2% of the ionizing luminosity and is unlikely to contribute significantly towards AGN feedback (King 2003).

This research has made use of data obtained from the High Energy Astrophysics Science Archive Research Center (HEASARC), provided by NASA's Goddard Space Flight Center. R.M.S. acknowledges support from NASA through the *Suzaku* and *Chandra* programs. M.E. thanks the NSF for support via grant AST-0807993. We would like to thank Tahir Yaqoob for assistance with the Chandra data analysis.

REFERENCES

- Ballantyne, D.R. 2005, MNRAS, 362, 1183
- Blandford, R.D. & Payne, D.G. 1982, MNRAS, 199, 883
- Blustin, A. J., Page, M. J., Fuerst, S. V., Branduardi-Raymont, G., & Ashton, C. E. 2005, A&A, 431, 111
- Cash, W. 1979, ApJ, 228, 939
- Chartas, G., Brandt, W. N., & Gallagher, S. C., 2003, ApJ, 595, 85
- Chartas, G., Brandt, W. N., Gallagher, S. C., & Garmire, G. P., 2002, ApJ, 579, 169
- Crenshaw, D. M., Kraemer, S. B., & George, I. M. 2003, ARA&A, 41, 117
- Dickey, J. M. & Lockman, F. J. 1990, ARA&A, 28, 215
- Eracleous, M., Halpern, J. P., & Charlton, J. C. 2003, ApJ, 582, 633
- Eracleous, M., & Halpern, J. P. 1994, ApJS, 90, 1
- Evans, D.A., et al. 2006, ApJ, 642, 96
- George, I. M., Turner, T. J., Netzer, H., Nandra, K., Mushotzky, R. F., & Yaqoob, T. 1998, ApJS, 114, 73
- Gelderman, R. & Whittle, M. 1994, ApJS, 91, 491
- Glozzi, M., Sambruna, R. M., Eracleous, M., & Yaqoob, T. 2007, ApJ, 664, 88
- Grevesse, N. & Sauval, A. J. 1998, Space Sci. Rev., 85, 161
- Kallman, T. R., Palmeri, P., Bautista, M. A., Mendoza, C., & Krolik, J. H. 2004, ApJS, 155, 675
- Kaspi, S., Netzer, H., Chelouche, D., George, I. M., Nandra, K., & Turner, T.J. 2004, ApJ, 611, 68
- Kellermann, K. I., Sramek, R., Schmidt, M., Shaffer, D. B., & Green, R. 1989, AJ, 98, 1195
- King, A. R., & Pounds, K. A. 2003, MNRAS, 345, 657
- King, A. R. 2003, ApJ, 596, L27

- Koski, A. 1978, *ApJ*, 223, 56
- Lawson, A. & Turner, M. J. L. 1997, *MNRAS*, 288, 920
- Marchesini, D., Celotti, A., & Ferrarese, L. 2004, *MNRAS*, 351, 733
- McKernan, B., Yaqoob, T., & Reynolds, C. S. 2007, *ApJ*, 379, 1359
- Porquet, D., Reeves, J.N., O’Brien, P.T., & Brinkmann, W. 2004, *A&A*, 422, 85
- Pounds, K. A., Reeves, J. N., King, A. R., Page, K. L., O’Brien, P. T., & Turner, M. J. L. 2003, *MNRAS*, 345, 705
- Reeves, J. N., Done, C., Pounds, K. A., Terashima, Y., Hayashida, K., Anabuki, N., Uchino, M., & Turner, M. J. L. 2008, *MNRAS*, 385, L108
- Reeves, J. N., O’Brien, P. T., & Ward, M. J., 2003, *ApJ*, 593, L65
- Reynolds, C.S. 1997, *MNRAS*, 286, 513
- Sambruna, R. M., Reeves, J. N., & Braitto, V. 2007, *ApJ*, 665, 1030
- Spergel, D. N., et al. 2003, *ApJS*, 148, 175
- Torresi, E., Grandi, P., Guainazzi, M., Palumbo, G. G. C., Ponti, G., & Bianchi, S. 2009a, *A&A*, 498, 61
- Torresi, E., Grandi, P., Longinotti, A., Guainazzi, M., Palumbo, G. G. C., Tombesi, F., & Nucita, A. 2009b, *MNRAS*, submitted, arXiv0907.0405
- Wilkes, B. J. & Elvis, M. 1987, *ApJ*, 323, 243

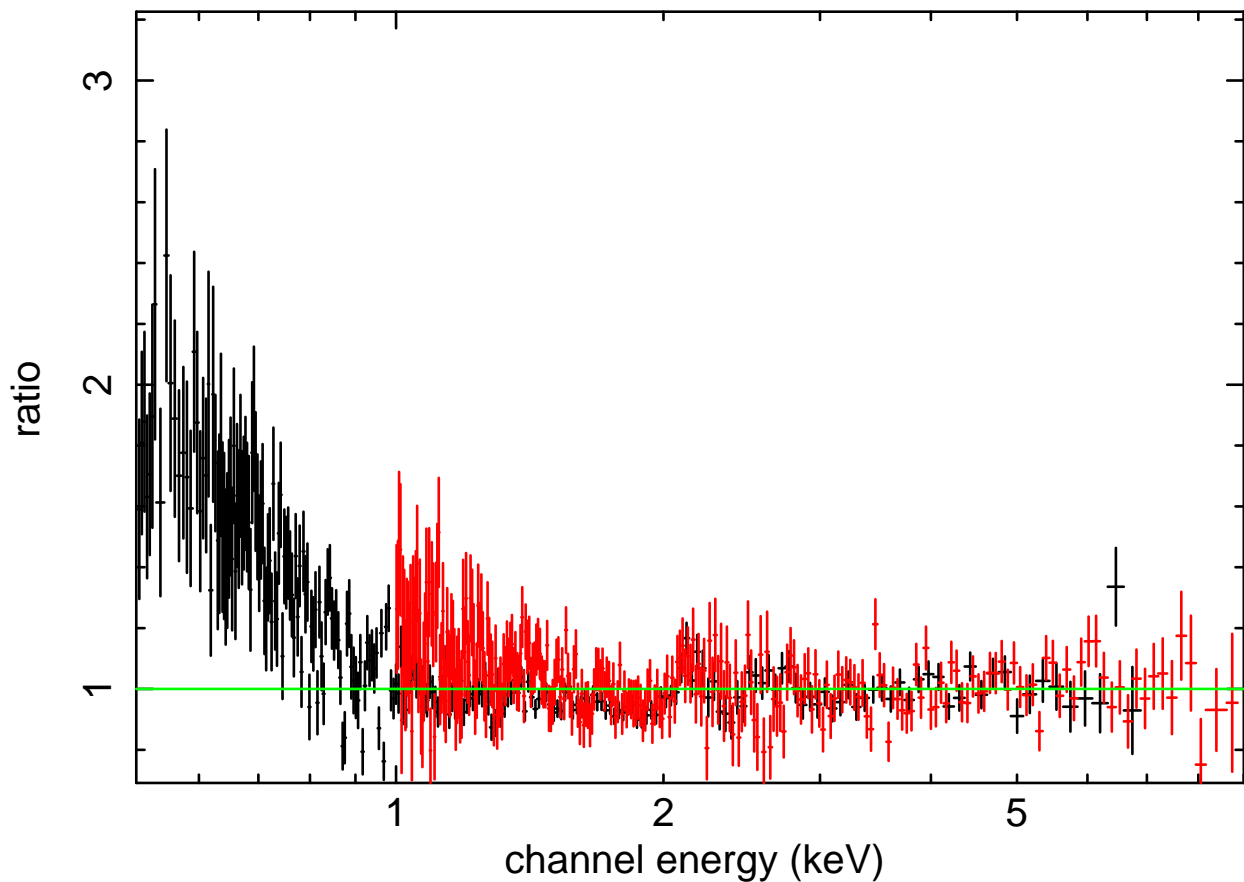


Fig. 1.— Chandra HETG MEG (black) and HEG (red) spectra of 3C 382, binned coarsely at four times the resolution of the gratings, in order to show the broad-band continuum spectrum. The data is plotted as a ratio against an absorbed power-law, of photon index $\Gamma = 1.66$. A clear excess of counts is present in the soft X-ray band below 1 keV, while significant residuals below unity are also present between 0.7–1.0 keV, indicating that a warm absorber is present.

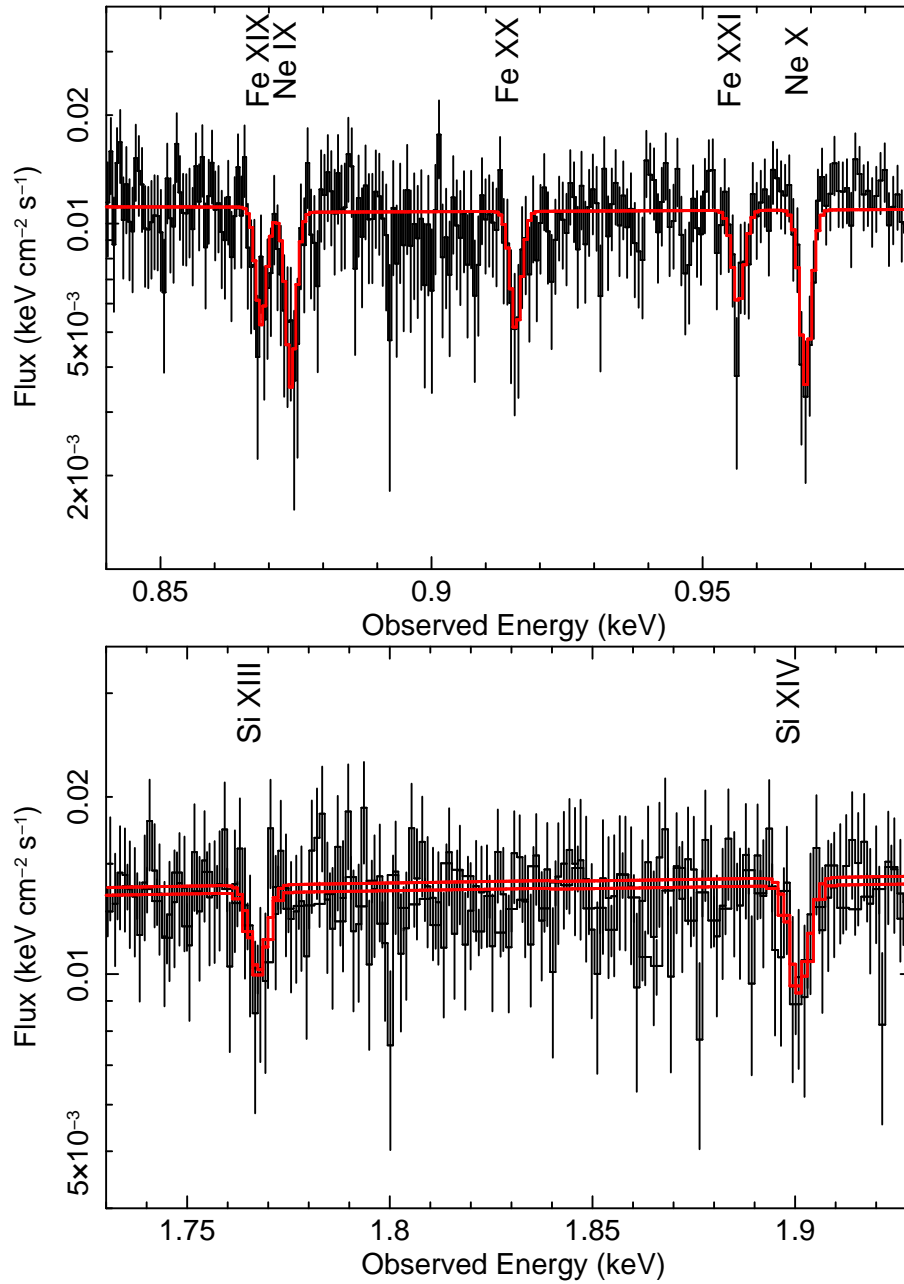


Fig. 2.— Fluxed HETG spectra showing the comparison between the data binned at HWHM resolution and the best-fit absorption line model (solid line) described in the text. Several absorption lines are present in the HETG spectrum, as labelled in the above figure and listed in Table 1.

Table 1. Summary of HETG absorption line parameters.

E(obs) ^a	E(rest) ^b	ID ^c	EW ^d	v_{out}^e	σ^f	ΔC^g
868.5	918.8 ^{+1.1} _{-0.9}	Fe XIX $2p - 3d$ (917.0)	-1.4 ± 0.5	590 ⁺³⁶⁰ ₋₂₉₀	509 ⁺⁴⁷⁰ ₋₂₁₆	24
874.1	924.7 ^{+0.6} _{-0.7}	Ne IX $1s - 2p$ (922.0)	$-1.9^{+0.5}$ _{-0.4}	875 ⁺¹⁹⁵ ₋₂₃₀	493 ⁺³⁵⁷ ₋₂₀₀	35
915.8	968.8 ^{+0.5} _{-0.9}	Fe XX $2p - 3d$ (967.3)	-1.6 ± 0.5	460 ⁺¹⁶⁰ ₋₂₈₀	516 ⁺⁴⁹⁰ ₋₄₀₀	21
956.6	1012.0 ^{+0.7} _{-0.7}	Fe XXI $2p - 3d$ (1009.0)	$-1.4^{+0.4}$ _{-0.5}	890 \pm 210	296 ⁺⁴⁰⁰ ₋₇₁	19
969.0	1025.1 ^{+0.4} _{-0.4}	Ne X $1s - 2p$ (1021.5)	$-2.1^{+0.4}$ _{-0.5}	1050 \pm 120	289 ⁺¹¹⁴ ₋₁₀₂	48
1767.7	1870.0 ^{+1.2} _{-1.3}	Si XIII $1s - 2p$ (1865.0)	$-1.6^{+0.4}$ _{-0.6}	800 ⁺¹⁹⁰ ₋₂₁₀	255 ⁺²⁷² ₋₁₆₅	26
1901.1	2011.1 ^{+0.3} _{-1.2}	Si XIV $1s - 2p$ (2004.4)	-2.2 ± 0.7	1000 ⁺⁵⁰ ₋₁₈₀	284 ⁺³⁰⁸ ₋₁₈₀	32
1281.4	1355.6 ^{+1.0} _{-1.0}	Mg XI $1s - 2p$ (1352.2)	-1.0 ± 0.4	750 \pm 220	340 ^h	12
1395.4	1476.2 ^{+1.0} _{-1.0}	Mg XII $1s - 2p$ (1472.2)	-0.8 ± 0.4	810 \pm 203	340 ^h	9

^aObserved energy of absorption line in eV.

^bEnergy of absorption line in rest-frame of 3C 382, in units eV.

^cline identification and lab frame energy in eV in parenthesis. Atomic data are from <http://physics.nist.gov>

^dEquivalent width, units eV.

^eOutflow velocity of absorption line, in units km s^{-1} .

^f 1σ velocity width of absorption line, in units km s^{-1} .

^gImprovement in C-statistic, upon adding line to model.

^hParameter is fixed in the model.